Image potential states at transition metal oxide surfaces: A time-resolved two-photon photoemission study on ultrathin NiO films

K. Gillmeister,[1] M. Kiel,[1] and W. Widdra[1,2]
[1]*Institut für Physik, Martin-Luther-Universität Halle-Wittenberg, Halle, Germany*
[2]*Max-Planck-Institut für Mikrostrukturphysik, Halle, Germany*

(Received 3 June 2015; revised manuscript received 15 February 2017; published 16 February 2018)

For well-ordered ultrathin films of NiO(001) on Ag(001), a series of unoccupied states below the vacuum level has been found. The states show a nearly free electron dispersion and binding energies which are typical for image potential states. By time-resolved two-photon photoemission (2PPE), the lifetimes of the first three states and their dependence on oxide film thickness are determined. For NiO film thicknesses between 2 and 4 monolayers (ML), the lifetime of the first state is in the range of 28–42 fs and shows an oscillatory behavior with increasing thickness. The values for the second state decrease monotonically from 88 fs for 2 ML to 33 fs for 4 ML. These differences are discussed in terms of coupling of the unoccupied states to the layer-dependent electronic structure of the growing NiO film.

DOI: 10.1103/PhysRevB.97.085424

I. INTRODUCTION

Image potential states (IPS) form a special class of surface states, in which electrons are bound in front of a polarizable surface. In response to electrons on the vacuum side, polarization charges are induced at the surface region of the bulk. They result in an attractive image potential that can bind the electrons perpendicularly to the surface. Since the first substantiation of image potential states by 2PPE in 1985 [1], this method is nowadays the tool of choice for such investigations. IPS play a decisive role as model systems to study fundamental decay processes of excited electrons. Extensive research has been conducted on IPS on bare metal surfaces [2–9], metal layers on metals [10–12], rare gas adlayers on different metallic substrates [13–20], and organic thin films on metal surfaces [21–27].

Albeit IPS are exclusive surface states, they can provide information about the electronic structure of the surface to which they couple. IPS can be modified by the (surface projected) bulk band structure [16,17] and will be transformed into resonances by interacting with electronic states at similar energies, as has been also shown for quantum-well states [12,27]. Strong interactions might even suppress IPS completely [8].

Theoretically, IPS are well understood and the dynamics of electrons in IPS are described well [28–30]. IPS of bare metal surfaces are often treated in the bulk penetration model. The decay processes of electrons in IPS are determined by their interaction with bulk electrons [12]. Larger lifetimes are found for lower penetration of the IPS wave function into the bulk, and vice versa. In addition, one has to consider the influence of the long-range Coulomb interaction as it influences the available phase space for decay processes strongly [28,31].

IPS of metal surfaces can be decoupled with the help of insulating adsorbate layers [17]. Thereby, the decoupling is most effective for adlayers that do not introduce any electronic states in the energy region of the IPS. The lifetime of IPS in such systems can be one or two orders of magnitude longer than for clean metal surfaces depending on the morphology and electronic structure of the adlayers [17].

Up to now, only a few 2PPE investigations on metal oxides have been reported, whereas none of these investigations focuses on image potential states and their lifetimes [32–37]. For transition-metal oxides with a static dielectric constant ε_0 in the range of 4–12, one expects again a series of IPS converging to the vacuum level as electrons in these states introduce polarization charges at the oxide surface. However, the exact position and especially the lifetime of the IPS depend on the presence of oxide conduction band states below the vacuum level. Here we present a 2PPE study of IPS for ultrathin epitaxial films of the charge-transfer insulator NiO grown pseudomorphically on Ag(001) in the thickness range between 2 and 4 ML.

NiO has a fundamental band gap of about 4 eV starting at 1.5 eV below E_F for bulk NiO and NiO films on Ag(001) [38–40] as sketched in Fig. 1(b) and determined by photoemission and inverse photoemission. The Ag(001) substrate exhibits a band gap around the $\overline{\Gamma}$ point that extends from 2 to 6.8 eV above E_F [41,42] as is schematically indicated in Figs. 1(a) and 1(b). For ultrathin NiO films, however, one expects a modified and thickness-dependent band structure due to electron confinement within the oxide film and due to the vicinity of the metal-oxide interface. With increasing thickness it will finally converge to the NiO bulk electronic structure [43,44]. At the NiO surface, one expects a series of IPS (labeled states 1 and 2 in Fig. 1, indicated in red) below the vacuum level. In the following, we present data for long-living

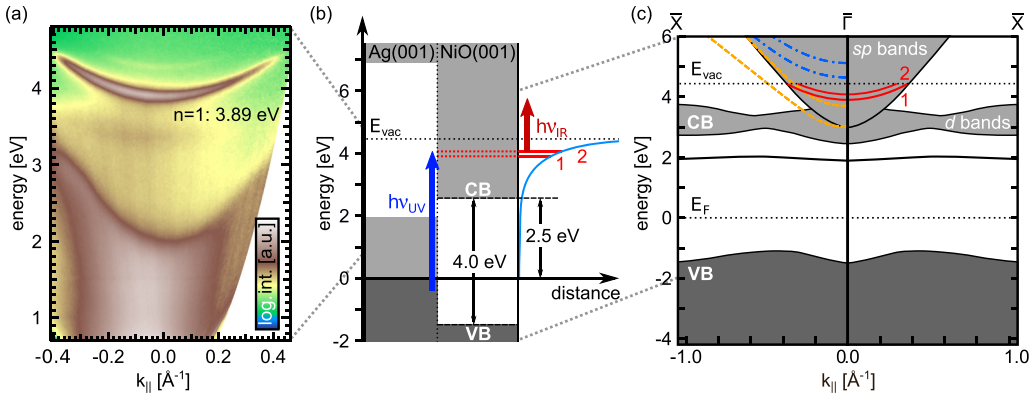

FIG. 1. Band alignment of NiO(001)/Ag(001): (a) 2PPE measurement of the projected band structure of the unoccupied states of Ag(001) in $\overline{\Gamma X}$ direction using $h\nu_{\mathrm{UV}} = 4.41$ eV. The $n = 1$ IPS of Ag(001) is located at $E_{\mathrm{int}} = 3.89$ eV. (b) Energy level scheme of the system NiO(001)/Ag(001) at the $\overline{\Gamma}$ point including the image potential (blue solid line). The unoccupied states 1 and 2 are pumped by $h\nu_{\mathrm{UV}}$ and probed by $h\nu_{\mathrm{IR}}$. (c) Schematic surface-projected bulk band structure of NiO [45] with an energy-shifted conduction band to fit the experimental band gap of 4 eV [38]. In the energy range of interest the theoretical calculations yield *sp*-derived unoccupied states localized at the surface (dashed orange and dashed-dotted blue lines).

unoccupied states near the vacuum level that are assigned to NiO image potential resonances. Depending on the NiO film thickness in the range between 2 and 4 ML, we find different lifetimes and effective masses of these states that are discussed with respect to coupling to quantum-well and conduction band states. In this way, the present study extends the discussion of IPS to the field of transition metal oxides, where NiO is the prominent example for a strongly correlated oxide.

II. EXPERIMENTAL DETAILS

Sample preparation and all experiments have been performed in an ultrahigh vacuum (UHV) chamber working at a base pressure of 1×10^{-10} mbar. The chamber is equipped with an optics for low energy electron diffraction (LEED), an x-ray source for x-ray photoelectron spectroscopy (XPS), as well as a UV source for ultraviolet photoelectron spectroscopy (UPS). The photoemitted electrons are detected by a hemispherical analyzer (Phoibos 150, SPECS, Germany) which contains a CCD detector for simultaneous recording of electron energy and emission angle ϑ. For 2PPE, a broadly tunable femtosecond laser system is used that includes two noncollinear optical parametric amplifiers which are pumped by a 20 W all-fiber laser (IMPULSE, Clark) as described elsewhere [46,47]. For the experiments described here, UV laser pulses with an energy of 4.17–4.27 eV for optical pumping are combined with infrared (IR) laser pulses (1.68–1.72 eV) for probing with typical pulse lengths of 50–90 fs and 35–45 fs, respectively. In time-resolved experiments, energy-resolved 2PPE spectra are taken for different time delays between pump and probe pulses ($\Delta t = 5$ fs). The cross correlation as well as the time zero between pump and probe pulses are determined simultaneously with the decay of the IPS from the two-dimensional $E(k)$ data. For this purpose, Gaussian fits of the transient 2PPE signals at about 0.5 eV above the low-energy cutoff are used where no long-living unoccupied states are observed [48]. If not stated otherwise, all reported electron energies are referenced to the Fermi energy $E_F = 0$.

The Ag(001) crystal was cleaned by several cycles of Ar ion sputtering and subsequent annealing at 600 K until no contamination could be detected by XPS. NiO ultrathin films have been grown via molecular beam epitaxy (MBE) as established by Marre and Neddermeyer [49–51]. Thereby, Ni was evaporated from a Ta crucible in an oxygen atmosphere of 2×10^{-6} mbar with a total growth rate of 0.5 ML/min. NiO films of 2, 3, and 4 ML thickness have been prepared and subsequently annealed at 540 K to improve long-range order and film perfection. The quality of the films has been monitored by the sharpness of the LEED spots [cf. Fig. 2(a)]. As reported also earlier, we find a layer-by-layer growth for NiO on Ag(001) [51–54] for thicknesses starting at 2 ML. Hence, after calibrating the evaporator it was possible to prepare well-ordered NiO layers with an accuracy of $\pm10\%$ in thickness.

A combination of LEED, XPS, and work function measurements based on photoemission onset has been used for calibration of the NiO film thickness. In the monolayer regime, NiO shows a (2×1) structure [50,52,53,55,56]. It is formed by a uniaxially distorted, nearly planar, quasihexagonal NiO structure [55]. Above 1 ML, the (2×1) super cell vanishes and a pseudomorphic rocksaltlike (1×1) structure is formed [53,57]. In Fig. 2(a), diffraction patterns of 1–4 ML NiO/Ag(001) are displayed. Intensity profiles along the $\overline{\Gamma X}$ direction give clear evidence that the (2×1) diffraction spots only appear for the NiO monolayer [Fig. 2(b)]. Figure 2(c) depicts the intensity of the (2×1) LEED spots with increasing coverage (left axis). For the completed monolayer, the (2×1) intensity is maximal. The structural transition from a quasihexagonal monolayer to rocksaltlike NiO films starting from 2 ML on leads to the disappearance of the (2×1) spots in LEED. Note that thicker NiO(001) films do show a *magnetic* (2×1) superstructure that is, however, visible in LEED only at selected electron kinetic energies.

Due to the quasihexagonality, the chemical environment as well as the resulting surface dipole of the NiO monolayer is different from those of thicker films. These issues lead to unique features in photoelectron spectra [55,57] and to a high

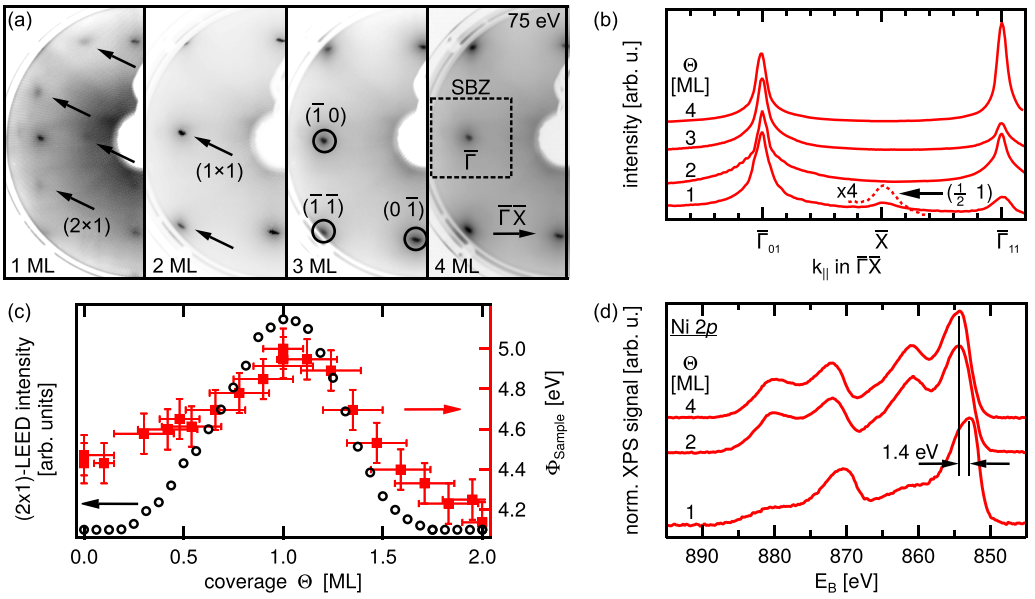

FIG. 2. (a) Diffraction patterns of annealed NiO films on Ag(001) with thicknesses of 1–4 ML at 75 eV electron energy. The appearing diffraction spots, the surface Brillouin zone (SBZ), as well as the $\overline{\Gamma X}$ direction are denoted. (b) Intensity profiles across the LEED images along the $\overline{\Gamma X}$ direction of the SBZ. (c) LEED intensity of the (2×1) spots (black open circles, left scale) and work function Φ as measured by UPS (red solid squares, right scale), respectively, vs NiO coverage for an as-prepared sample. (d) XP spectra of the Ni2p core levels for 1, 2, and 4 ML NiO/Ag(001). All spectra are normalized to their maximum and shifted in intensity for the sake of clarity.

work function with respect to other coverages. In Fig. 2(d) XP spectra of the Ni 2p core level are depicted for NiO films from 1–4 ML thickness. While the spectra for 2 and 4 ML are similar and even bulklike in shape [58,59], the spectrum for 1 ML NiO/Ag(001) differs significantly: The maximum of the Ni $2p_{3/2}$ peak appears with a difference of 1.4 eV at lower binding energy, and the satellite structure is differently shaped in comparison to the spectra for higher coverages. This is in accordance with findings in the literature [55,57] and can be taken as a marker for this thickness.

In Fig. 2(c) the work function is plotted as function of the oxide film thickness. For 1 ML it shows a characteristic maximum of $\Phi_{\mathrm{ML}} \sim 5.0$ eV. This value differs strongly from that of clean Ag(001) ($\Phi_{\mathrm{Ag}} \sim 4.5$ eV) and these of thicker films ($\Phi_{\mathrm{NiO}} \sim 4.2$–$4.4$ eV). Therefore, one can clearly identify one monolayer also on the basis of work function measurements.

III. RESULTS

In Fig. 3 2PPE spectra for two different preparations of 2 ML NiO/Ag(001) are depicted for fixed time delays Δt between pump (UV) and probe (IR) pulse. The spectra of Fig. 3(a) were obtained directly after film preparation at room temperature (RT) using photon energies of 4.27 and 1.68 eV for pump and probe, respectively. Four different features are identified in the spectra for time delays of $\Delta t = 0$ and 115 fs. Long-living states dominate the spectrum at $\Delta t = 115$ fs and are marked with 1, 2, and 3 in Fig. 3(b). These features correspond to energies of 3.78, 4.04, and 4.14 eV (each ±0.05 eV) above E_F in Fig. 3(a). A fourth short-living feature, tagged with B, is located at 3.91 eV.

The spectra of Fig. 3(b) were measured with photon energies of 4.17 (pump) and 1.72 eV (probe beam) after annealing the sample at 540 K. Again, the spectra can be described by four different states at energies of 3.75, 4.05, 4.14, and 3.90 eV (B). In contrast to the measurement directly after RT preparation, the spectra are dominated by feature 1 for both time delays Δt. Due to the reduced pump photon energy of 4.17 eV, state 3 is hardly populated and almost not visible in the spectra.

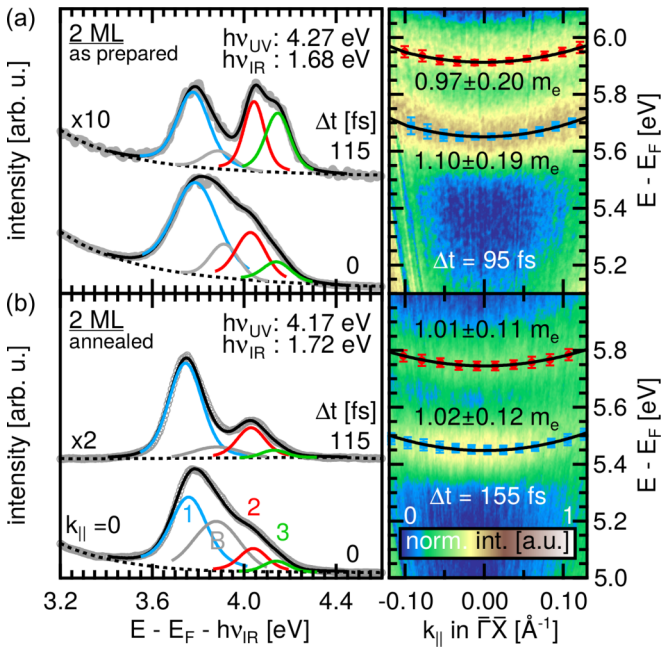

FIG. 3. 2 ML NiO/Ag(001): 2PPE spectra at $k_{\parallel} = 0$ (left panel) and momentum-resolved data (right panel). The data have been measured (a) directly after film preparation and (b) after annealing at 540 K for time delays of $\Delta t = 0$ and $\Delta t = 115$ fs, respectively. The as-prepared (annealed) sample was pumped with $h\nu_{\mathrm{UV}} = 4.27$ eV (4.17 eV) and probed with $h\nu_{\mathrm{IR}} = 1.68$ eV (1.72 eV).

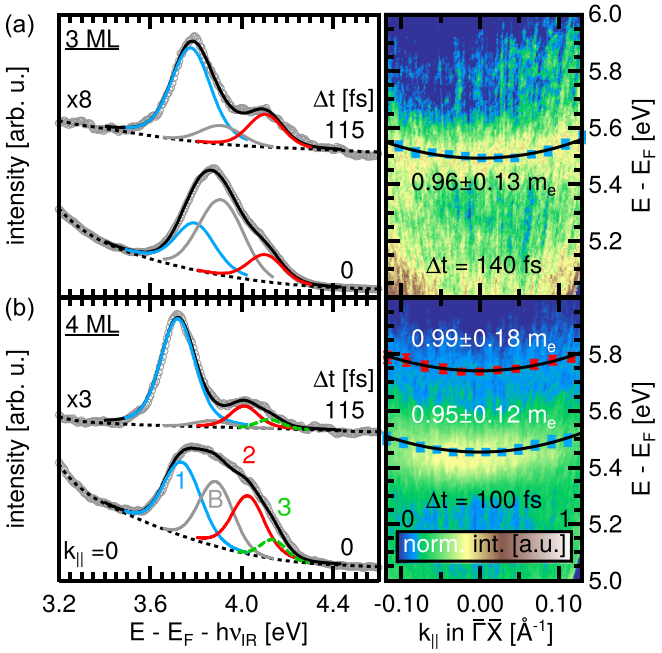

FIG. 4. 2PPE spectra for $k_{\parallel} = 0$ (left panel) and momentum-resolved data (right panel) for 3 ML (a) and 4 ML (b) NiO/Ag(001), pumped with $h\nu_{UV} = 4.17$ eV and probed with $h\nu_{IR} = 1.72$ eV at different time delays Δt.

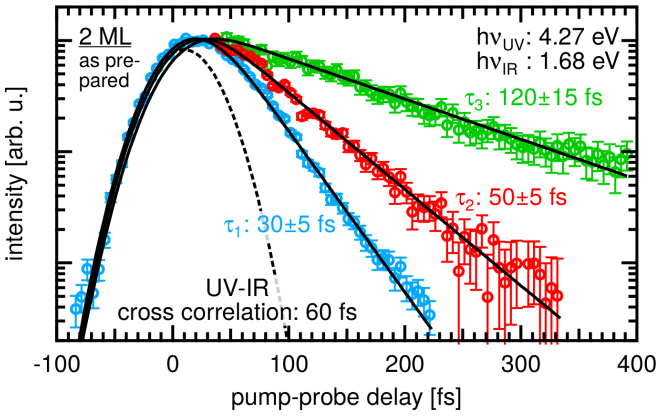

FIG. 5. Time-dependent 2PPE intensities (data points) of the features 1 (blue, bottom), 2 (red, middle), and 3 (green, top) for the as-prepared 2 ML NiO/Ag(001). The intensities are described by rate equations resulting in the decay curves (black solid lines) which yield the denoted well-defined lifetimes. The dashed black line represents the cross correlation between UV and IR pulses.

Momentum-resolved data (right panel in Fig. 3) reveal a dispersion of the states 1 and 2 with effective masses for the as-prepared (annealed) sample of $m_{\text{eff}} = 1.1\ (1.02)\ m_e$ for feature 1 and 0.97 (1.01) m_e for feature 2, respectively. In other words, both states show a free-electron-like dispersion parallel to the sample surface.

For 3 and 4 ML NiO/Ag(001), similar unoccupied states are found (Fig. 4). The energies of these features are 3.79, 4.11 for the first and second state and 3.90 eV (B) for 3 ML [60]. They shift to 3.73, 4.02 (1, 2) and 3.89 eV (B) for 4 ML (each ±0.05 eV). The energetic positions of these unoccupied states differ only slightly from those of the 2 ML states. The features show a dispersion (right panel in Fig. 4) with effective masses m_{eff} of 0.96, 0.95 (feature 1), and 0.99 m_e (feature 2). In addition, one can again recognize a short-living feature B as has been seen for 2 ML.

In Table I these data are summarized together with the sample work functions Φ obtained by UPS. For the as-prepared bilayer, the work function Φ amounts to 4.18 eV and is about 250 meV lower than for the annealed NiO films with 2–4 ML thickness. This difference is explained according to the Smoluchowski effect [61] by a higher step density for the as-prepared NiO film.

The analysis of the 2PPE data was done as follows. The raw data (CCD images) were measured by tuning the temporal overlap between pump (UV) and probe (IR) beam. From the raw CCD detector images energy-resolved intensity profiles around a photoemission polar angle of 0 deg with an angular width of 4 deg were extracted and used as spectra for the analysis. For delays far from the temporal overlap of both laser pulses, a spectrum only consists of the single contributions of the UV and the IR beam, respectively. These so called single color contributions were subtracted from each spectrum and for each time delay in a first step. Second, the photoemission background due to secondary electron processes was subtracted (black dotted lines in Figs. 3 and 4). The double-corrected spectra were then fitted using Voigt profiles for all time delays between UV and IR, generating the time-dependent intensity of each single Voigt profile (data points in Figs. 5 and 6).

In Fig. 5 time-dependent 2PPE intensities for the features 1–3 are depicted for the as-prepared 2 ML NiO(001) film. The data points are fitted using a rate equation approach (black solid lines). For comparison, the cross correlation curve between pump and probe pulse which has been determined simultaneously and which has a full width at half maximum (FWHM) of 60 fs is also included in Fig. 5. The solid lines describe the experimental data well over two and a half orders

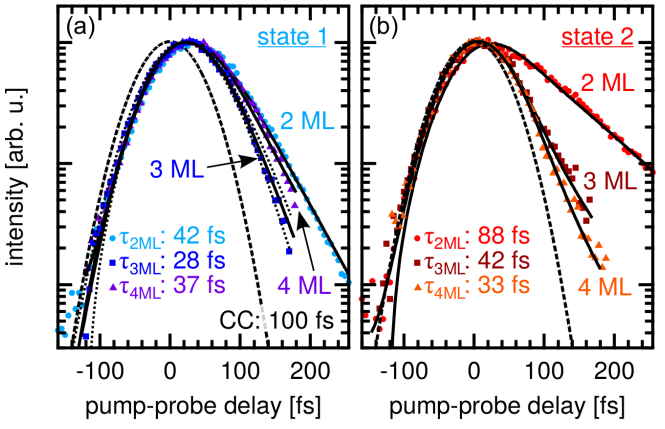

FIG. 6. Time-dependent 2PPE intensities (data points) of (a) state 1 (blue colors) and (b) state 2 (red colors) of annealed 2–4 ML NiO/Ag(001). For comparison, the cross correlation traces are depicted as dashed black lines. The dotted black lines in (a) are data fits resulting from −5 fs shorter and +5 fs longer lifetimes as compared to the best data fit for 3 ML (black solid line).

TABLE I. Intermediate state energies E_{int}, binding energies E_B, effective masses m_{eff}, and lifetimes τ of the first three image potential states for NiO(001) ultrathin films on Ag(001) with thicknesses between 2 and 4 ML. For comparison, data for the IPS on bare Ag(001) [47] are included (marked 0 ML). The second column gives the work functions Φ as measured by UPS. The uncertainties amount to ±50 meV for the given energies.

		State 1				State 2				State 3		
Coverage (ML)	Φ (eV)	E_{int} (eV)	E_B (meV)	m_{eff} (m_e)	τ (fs)	E_{int} (eV)	E_B (meV)	m_{eff} (m_e)	τ (fs)	E_{int} (eV)	E_B (meV)	τ (fs)
0 [47]	4.43		561		57		170		165		72	380
2[a]	4.18	3.78	400	1.10 ± 0.19	30 ± 5	4.04	120	0.95 ± 0.20	50 ± 5	4.14	40	120 ± 15
2[b]	4.44	3.75	690	1.02 ± 0.12	42 ± 6	4.05	390	1.01 ± 0.11	88 ± 18	4.14		
3[b]	4.43	3.79	640	0.96 ± 0.13	28 ± 5	4.11	320		42 ± 14			
4[b]	4.41	3.73	680	0.95 ± 0.12	37 ± 8	4.02	390	0.99 ± 0.18	33 ± 13	(4.14)		

[a]As-prepared.
[b]Annealed to 540 K.

of magnitude in intensity and yield lifetimes of 30 ± 5, 50 ± 5, and 120 ± 15 fs for the three states.

For the annealed 2 ML film, the lifetimes (Fig. 6) differ significantly from those of the as-prepared film. The lifetime of feature 1 is about 12 fs longer (42 ± 6 fs), whereas the lifetime of feature 2 has increased by 38 fs (to 88 ± 18 fs). In Fig. 6 a comparison of the time-resolved 2PPE data for 2, 3, and 4 ML (all annealed to 540 K) is presented. The fits yield lifetimes of 28 ± 5 and 37 ± 8 fs for state 1 of 3 and 4 ML. The lifetimes of state 2 for 3 and 4 ML amount to 42 ± 14 and 33 ± 13 fs, respectively.

Despite a relatively large pump-probe cross correlation of 100 fs (cf. Fig. 6), the lifetimes of the unoccupied states can be determined with an accuracy down to ±5 fs due to the *in situ* determination of time zero and cross correlation. During the fitting process, the uncertainties of the time zero *and* of the cross correlation were included as constraints [48]. In Fig. 6(a), the comparison of lifetime fits with 28 fs (solid line) and with 5 fs shorter as well as longer lifetimes (dotted lines) demonstrates the lifetime accuracy which is similar to previous studies [4].

The lifetime of feature B at about 3.9 eV (cf. Figs. 3 and 4) has been found to be lower than 15 fs. A discussion of this fast-decaying state is carried out at the end of the following section.

IV. DISCUSSION

Figure 1 depicts the projected band structures of Ag(001) and NiO(001) as well as their alignments. For bare Ag(001), momentum-resolved 2PPE data are shown in Fig. 1(a). One can recognize the strongly dispersing unoccupied *sp* bulk bands which extend at $k_{\parallel} = 0$ to ~2 eV above E_F. It defines the lower edge of the Ag(001) band gap at the $\overline{\Gamma}$ point which reaches well above the vacuum level [41,42,62]. Additionally, the first two image potential states at 3.89 and 4.25 eV above E_F are well reproduced in good agreement with recent studies [2,4,47,63].

The electronic structure of NiO(001) and NiO(001)/Ag(001) in the energy region near E_F has been investigated by photoemission and inverse photoemission spectroscopy [38,40,64–66]. In these studies, the valence band maximum has been found at 1.5–2 eV below E_F for bulk NiO which fits to our UPS data (not shown here). On the other hand, the onset of inverse photoemission features has been assigned to the NiO conduction band (CB) which is formed by the Ni3*d* upper Hubbard band. This defines the ~4 eV fundamental band gap of bulk NiO. Theoretical studies of the NiO band structure support this assignment and emphasize the strong effect of electron correlation [45,67–69]. The surface-projected band structure for bulk NiO along the $\overline{\Gamma X}$ direction as adapted from Schrön *et al.* [45] and shifted according to the experimentally determined NiO band gap is sketched in Fig. 1(c). The NiO CB starts at 2.5 eV and is formed by localized Ni3*d* states, whereas O-derived states form stronger dispersing *sp* bands centered around $\overline{\Gamma}$ at higher energies [45].

All experiments described here use laser pulses with photon energies of 4.2–4.3 eV for the primary photoexcitation process. In principle, these photon energies enable excitation across the band gap of NiO. Such excited electrons could populate states up to 2.7 eV above E_F only due to the location of the valence band maximum at 1.5 eV below E_F. In contrast, the photoelectrons close to the vacuum level that are the subject in the present paper are at higher energies and are, therefore, pumped from metallic substrate states in the energy region slightly below the Fermi level as indicated by the blue arrow in Fig. 1(b). Note that the photon energies of the infrared probe pulses are too low for any primary photoexcitation.

The position and the dispersion of the experimentally observed unoccupied states for 2–4 ML NiO/Ag(001) are depicted in Fig. 1(c) as red parabolae. For comparison, the calculated states of the *sp*-derived bands that exhibit surface state or surface resonance character are indicated on the left-hand side [45]. They disperse with effective masses of about 0.6 m_e (orange dashed lines) and nearly 1 m_e (blue dashed dotted lines) [45]. Inside the charge-transfer gap of NiO, a barely dispersing surface state is located around 2 eV above E_F (black line).

In the 2PPE experiments, we find a series of three unoccupied states converging towards the vacuum level in the energy range between 3.5 and 4.4 eV above E_F. In Table I their intermediate state energies E_{int} with respect to the Fermi level, binding energies E_B with respect to the vacuum level, effective masses m_{eff}, and lifetimes τ are summarized for 2, 3, and 4 ML of NiO(001) on Ag(001). Data for the work function (adopted by UPS) and the IPS on bare Ag(001) (marked 0 ML coverage) [47] are included for comparison.

In the following we discuss the three unoccupied states in three steps. First, we rule out a possible observation of pure unoccupied NiO bulk states. Second, we assign them to image potential resonances. The discussion is, finally, followed up by comments on the interaction of image potential and quantum-well states that develop inside the NiO film.

(i) NiO conduction band states are expected in the energy range of the observed unoccupied states [cf. Fig. 1(c)]. In fact, the theoretical study of Schrön *et al.* predicts flat unoccupied d bands and stronger dispersing unoccupied sp bands. While the band dispersions are theoretically described well, the absolute energies of the calculated unoccupied states have to be taken with care. Besides a d_{z^2} derived unoccupied surface state around 2 eV, distinct sp-derived NiO(001) states at 3.0 and 3.70 eV ($m_{\text{eff}} \sim 0.6\ m_e$) and at 4.67 and 5.14 eV ($m_{\text{eff}} \sim 1.0\ m_e$), respectively, are marked as dotted and dashed-dotted lines in Fig. 1(c). These states have an increased probability density at the surface. According to the excitation scheme depicted in Fig. 1(b) we have to consider a direct population of such NiO CB states by the pump pulse, i.e., a pure d or sp character of the found states.

All investigated 2PPE features show a dispersion with effective masses of about 1 m_e. Therefore, one can directly exclude a d-derived character of these states. In the same way, a pure sp character is also less likely: The observed features occur in the low energy range of the sp-derived NiO CB. Here the theoretically predicted CB states at 3.0 and 3.7 eV above the Fermi level could be addressed by the UV pump pulse. However, these NiO sp states disperse with effective masses of ~0.6 along the $\overline{\Gamma X}$ direction which are only one half of that of the investigated states. On the other hand, the theoretically predicted surface resonances at 4.67 and 5.14 eV [blue dashed-dotted in Fig. 1(c)] show effective masses of 1 m_e. However, their energies are well above the bottom of the sp-derived CB and are located to high with respect to the experimentally observed states.

As a consequence, the found 2PPE feature have to be characterized differently.

(ii) The image potential in front of a dielectric substrate is modified as compared with the situation in front of a metallic substrate by a factor β:

$$V(z) = -\frac{e^2}{4\pi\varepsilon_0}\frac{\beta}{4z}, \quad \beta = \frac{\varepsilon - 1}{\varepsilon + 1}, \tag{1}$$

where ε denotes the static dielectric constant and z is the distance from the dielectric surface. For an ultrathin film on a metal substrate, the finite thickness of the dielectric layer and the metallic response have additionally to be taken into account as discussed previously [70,71]

$$V(z) = -\frac{e^2}{4\pi\varepsilon_0}\left[\frac{\beta}{4z} - \frac{1-\beta^2}{4\beta}\sum_{k=1}^{\infty}\frac{(-\beta)^k}{z+kd}\right], \tag{2}$$

where d is the thickness of the dielectric layer. The first term of Eq. (2) describes the interaction between an electron and a dielectric layer, whereas the second term contains modifications of the dielectric response due to the metal underneath. For thick films *or* for β close to 1, the potential in front of the surface is dominated by the image potential of the dielectric. The dielectric constant for NiO of $\varepsilon = 12$ [72] yields $\beta = 0.85$ which is already close to one. Therefore, we expect only slightly modified binding energies for the IPS of NiO/Ag(001) as compared to the bare metal [71]. The binding energies E_n for a Rydberg-like series of electronic states converging to the vacuum level is given by $E_n = 0.85 \cdot \beta^2 m_{\text{eff}}/(n+a)^2$, where n is the quantum number of the state and a is the quantum defect. In case of nearly free electrons ($m_{\text{eff}} = 1$) in front of a metal ($\beta \to 1$), the largest possible binding energy for the first (second) IPS amounts to 850 (425) meV. The here observed binding energies of 640–690 meV for the first peaks as well as 320–390 meV for the second peaks (annealed films) fall therefore well in the energy range of IPS. The assignment of the 2PPE features to IPS is furthermore corroborated by the effective masses of these unoccupied states which are close to 1 m_e. In addition, the lifetimes of energetically higher lying features of 2 and 3 ML NiO/Ag(001) are longer as compared to lower lying ones (cf. Table I) following the general trend known from clean metals [73]. All of these findings are typical for IPS and support our interpretation.

Taking the band structure of the underlying NiO films into account [Fig. 1(b)] one recognizes that all features are in resonance with the NiO conduction band. Consequently, we have to consider them as image potential resonances (IPR).

As a result of a potentially resonant character the energies with respect to the Fermi level (IPR 1: 3.75 eV, IPR 2: 4.07 eV, IPR 3: 4.14 eV) change only slightly with NiO film thickness. The small variations by 50 meV for IPR 1 and 70 meV for IPR 2 can be explained by small differences in the strength of coupling.

(iii) The investigated system Ag(001)–NiO(001)–vacuum contains two interfaces: between the substrate and the dielectric film and between the film and the vacuum, respectively [Fig. 1(b)]. Energy barriers are formed on both sides of the NiO film due to the large energy gap between 2 and 7 eV in the band structure of Ag(001) on the one side and the vacuum on the other side. This leads to a break-up of the NiO CB and a formation of quantum-well states (QWS) inside the oxide film. Therefore, we have to consider a coupling of the IPS with such quantum-well states.

The interaction of IPS and QWS has been investigated previously [10,12,15–17,27]. Resonant coupling between IPS and QWS would lead to a lowering of the lifetime and, in accordance, to a significant increase of the binding energy of the IPR as has been investigated on rare gas adlayers on metal surfaces [16,17]. The coupling condition changes with increasing adlayer thickness according to the change of the width of the quantum well. This should be reflected in the lifetime and binding energy behavior of the coupled image potential states [15,16]. Furthermore, resonant coupling can even lead to a complete transition of states having image potential character to states with pure quantum well character. This is accompanied by an extensive broadening of the peak widths due to efficient coupling to the bulk [11,27].

For NiO(001) on Ag(001) we find an oscillatory behavior of the lifetime of the first IPR which is similar to, e.g., image potential states on Xe/Ag(111) [16]. Moreover, the lifetime of the second IPR decreases monotonically with increasing NiO film thickness comparable to 2PPE measurements on Xe/Cu(100) and Kr/Cu(100) [17]. Hence, our findings could be interpreted by the formation of quantum-well resonances

(a) at the energy of the first IPR for 3 ML and (b) at the energy of the second IPR for NiO film thicknesses $\geqslant$4 ML. However, the typical increase of the binding energies with increasing lifetime does not occur for the first nor for the second IPR (Table I). On the contrary, the binding energy *decreases* at 3 ML, whereas is nearly constant for the other NiO coverages without noticeable dependence on the lifetime. In addition, no significant broadening of the peaks is visible from the spectra in Figs. 3 and 4. Therefore, we assign the series of 2PPE features to image potential states that are weakly coupled to NiO bulk states.

The wave functions of the unoccupied states couple to states of the unoccupied *sp*-derived band of the NiO film which can be read from their energetic position [Fig. 1(c)] as well as their persistent dispersion with $m_e \sim 1$. The resonance between IP states and the NiO CB leads to a shift of their probability density towards the sample surface [17]. The resulting enhanced penetration of the wave function into the substrate explains the observed lifetime reduction from 57 fs (165 fs) of the $n = 1$ ($n = 2$) IPS of bare Ag(001) to 30–40 fs for the first IPR and <90 fs for the second IPR of annealed 2–4 ML NiO/Ag(001) due to an additional decay channel for resonant charge transfer into the bulk.

The electronic structure of the NiO(001)/Ag(001) thin film system may differ from the bulk band structure depicted in Fig. 1(c) and is varying with increasing film thickness, e.g., by formation of QW states. As a consequence, the coupling conditions between IPS and *sp*-derived states also vary. For example, the remarkably shorter lifetime of 28 fs for the first IPS of 3 ML NiO/Ag(001) points towards a stronger coupling of IPR to *sp*-derived states that evolve at this specific thickness. In a similar way, the different IPR lifetimes for the NiO layers are explained by modifications of the underlying electronic structure and, therefore, different coupling conditions. The lifetime of electrons from the second IPR decreases monotonically with increasing film thickness. For 4 ML, the lifetime of the second IPR electrons is even shorter than for electrons excited into the accordingly first IPR. This is explained by matching resonance conditions for the second IPR at 4 ML film thickness.

To promote our interpretations, detailed theoretical calculations on the layer-resolved band structure of the NiO films would be desirable. In addition, experiments on thicker NiO films would be helpful to get the transition from a thin film to a bulklike behavior.

One can recognize distinct variations between the data of the as-prepared 2 ML and the annealed 2 ML NiO films. According to the above interpretation of image-potential derived states, these differences can be assigned to the quality of the NiO films: The observed states for the as-prepared and the annealed 2 ML NiO films on Ag(001) differ only slightly in energy with respect to E_F (cf. Table I). In contrast, the binding energies of the features of the as-prepared sample as well as the work function are approximately 250 meV lower as compared to the annealed samples. This is interpreted within the concept of the local work function [10]. Work function measurements average over a large sample area containing flat NiO terraces as well as stepped NiO regions, resulting in a measured *global* work function. Electrons in an image potential state are located in front of the flat NiO terraces only. Therefore, they are affected by the *local* work function of the flat NiO regions. Since the energies of the IPR do not change for the as-prepared and annealed NiO bilayer, the local work function does not change for both preparations. Due to an enhanced film quality upon annealing the NiO bilayer, the global work function is close to that of the flat terraces for the annealed NiO bilayer. Hence, the correct binding energy of the IPR is reflected by the annealed bilayer.

The 12 fs shorter lifetime for the as-prepared 2 ML film in comparison to the film which has been annealed to 540 K demonstrates the influence of film imperfections on the IPR lifetime. As known from other systems, the electron dynamics strongly depend on defect and step densities [2,74–76]. These densities lead to a nonmomentum conserving scattering and, therefore, open up additional relaxation channels. For the annealed oxide films, the quality of the layers of different thicknesses as determined by the sharpness of the LEED spots [cf. Fig. 2(a)] is comparable. The film quality is significantly higher as compared to the as-prepared 2 ML film. Therefore, the IPR lifetimes for all annealed films should be less limited by surface imperfections. Usually, the second IPS is even more sensitive to the film quality as compared to the first IPS due to its longer lifetime and due to the possibility of nonmomentum conserving scattering into the first IPS. Indeed, the lifetime of the as-prepared 2 ML film is reduced to 50 in comparison to 88 fs for the annealed film.

In addition to the series of IPR, a short-living (<15 fs) unoccupied state B at about 3.9 eV above E_F has been observed for 2–4 ML NiO/Ag(001) (Figs. 3 and 4). Despite its origin is not yet fully clear, some statements regarding the character of this unoccupied state can be given. It is obvious that the intermediate energy of state B nearly coincides with that found for the $n = 1$ IPS of the clean Ag(001) substrate [3.89 eV, cf. Fig. 1(a)]. Therefore, it is most likely that feature B is a signal resulting from the $n = 1$ IPS of the silver substrate which occurs above remaining bare Ag patches at the sample surface. The substantially shorter lifetime of state B (max. 26% compared to the $n = 1$ IPS of clean Ag(001)) can be explained by enhanced scattering probability at residual Ni or O sites at the Ag patches. However, due to its energy position and its ultrashort lifetime, feature B can also be a candidate for the directly populated unoccupied O-derived *sp* state as mentioned above. The decay of such a bulklike state is much faster due to enhanced coupling of its wave function to the bulk compared to the spatially more decoupled image potential states.

V. CONCLUSIONS

We have investigated a series of unoccupied states for NiO(001) ultrathin films of 2–4 ML on Ag(001) in the energy range between 3.5 and 4.4 eV above E_F by means of angle- and time-resolved 2PPE. Regarding their energy position, their parabolic dispersion, and their lifetime behavior, they are assigned to image potential states resonant with NiO conduction band states. For the first IPR the lifetimes show an oscillatory behavior and differ only slightly for annealed NiO films with 2–4 ML thickness. In contrast, the lifetimes of the second IPR decrease with increasing film thickness from 88 (2 ML) to 33 fs (4 ML). This is explained by the presence of *sp*-derived NiO states in the energy range of the IPS which

lead to an enhanced layer-dependent coupling between NiO and IP states with increasing film thickness and thus to a faster decay compared to bare Ag(001). Additionally, the lifetime of the IPR depends strongly on the film quality as is demonstrated for a 2 ML NiO(001) film prepared at RT. Without annealing, the NiO bilayer yields significantly shorter lifetimes of the first and second IPR in comparison to an annealed film.

ACKNOWLEDGMENTS

The authors thank Ralf Kulla for generous technical assistance and Cheng-Tien Chiang for fruitful discussions. Financial support by the Deutsche Forschungsgemeinschaft via SFB 762 is gratefully acknowledged. K.G. thanks the International Max Planck Research School for Science and Technology of Nanostructures for funding.

[1] K. Giesen, F. Hage, F. J. Himpsel, H. J. Riess, and W. Steinmann, Two-Photon Photoemission via Image-Potential States, Phys. Rev. Lett. **55**, 300 (1985).

[2] S. Schuppler, N. Fischer, T. Fauster, and W. Steinmann, Bichromatic two-photon photoemission spectroscopy of image potential states on Ag(100), Appl. Phys. A **51**, 322 (1990).

[3] R. W. Schoenlein, J. G. Fujimoto, G. L. Eesley, and W. Capehart, Femtosecond photoemission studies of image potential and electron dynamics in metals, in *Laser Optics of Condensed Matter*, edited by E. Garmire, A. Maradudin, and K. Rebane (Springer, New York, 1991), pp. 71–82.

[4] I. L. Shumay, U. Höfer, Ch. Reuß, U. Thomann, W. Wallauer, and T. Fauster, Lifetimes of image-potential states on Cu(100) and Ag(100) measured by femtosecond time-resolved two-photon photoemission, Phys. Rev. B **58**, 13974 (1998).

[5] A. Schäfer, I. L. Shumay, M. Wiets, M. Weinelt, T. Fauster, E. V. Chulkov, V. M. Silkin, and P. M. Echenique, Lifetimes of unoccupied surface states on Pd(111), Phys. Rev. B **61**, 13159 (2000).

[6] S. Link, H. A. Dürr, and W. Eberhardt, Lifetimes of image-potential states on the Pt(111) surface probed by time-resolved two-photon photoemission spectroscopy, Appl. Phys. A **71**, 525 (2000).

[7] M. Marks, C. H. Schwalb, K. Schubert, J. Güdde, and U. Höfer, Quantum-beat spectroscopy of image-potential resonances, Phys. Rev. B **84**, 245402 (2011).

[8] M. Winter, E. V. Chulkov, and U. Höfer, Trapping of Image-Potential Resonances on a Free-Electron-like Surface, Phys. Rev. Lett. **107**, 236801 (2011).

[9] X. Cui, C. Wang, A. Argondizzo, S. Garrett-Roe, B. Gumhalter, and H. Petek, Transient excitons at metal surfaces, Nat. Phys. **10**, 505 (2014).

[10] R. Fischer, S. Schuppler, N. Fischer, T. Fauster, and W. Steinmann, Image States and Local Work Function for Ag/Pd(111), Phys. Rev. Lett. **70**, 654 (1993).

[11] R. Fischer and T. Fauster, Coupling of image states to quantum-well states for Au on Pd(111), Phys. Rev. B **51**, 7112 (1995).

[12] T. Fauster and W. Steinmann, Two-photon photoemission spectroscopy of image states, in *Electromagnetic Waves: Recent Developments in Research*, edited by P. Halevi (Elsevier, Amsterdam, 1995).

[13] D. F. Padowitz, W. R. Merry, R. E. Jordan, and C. B. Harris, Two-Photon Photoemission as a Probe of Electron Interactions with Atomically Thin Dielectric Films on Metal Surfaces, Phys. Rev. Lett. **69**, 3583 (1992).

[14] M. Wolf, E. Knoesel, and T. Hertel, Ultrafast dynamics of electrons in image-potential states on clean and Xe-covered Cu(111), Phys. Rev. B **54**, R5295 (1996).

[15] J. D. McNeill, R. L. Lingle, R. E. Jordan, D. F. Padowitz, and C. B. Harris, Interfacial quantum well states of Xe and Kr adsorbed on Ag(111), J. Chem. Phys. **105**, 3883 (1996).

[16] J. D. McNeill, R. L. Lingle, N.-H. Ge, C. M. Wong, R. E. Jordan, and C. B. Harris, Dynamics and Spatial Distribution of Electrons in Quantum Wells at Interfaces Determined by Femtosecond Photoemission Spectroscopy, Phys. Rev. Lett. **79**, 4645 (1997).

[17] W. Berthold, F. Rebentrost, P. Feulner, and U. Höfer, Influence of Ar, Kr, and Xe layers on the energies and lifetimes of image-potential states on Cu(100), Appl. Phys. A **78**, 131 (2004).

[18] J. Güdde and U. Höfer, Femtosecond time-resolved studies of image-potential states at surfaces and interfaces of rare-gas adlayers, Prog. Surf. Sci. **80**, 49 (2005).

[19] A. Hotzel, Electron dynamics of image potential states in weakly bound adsorbate layers: A short review, Prog. Surf. Sci. **82**, 336 (2007).

[20] A. Damm, K. Schubert, J. Güdde, and U. Höfer, Observation of the transition from image-potential states to resonances on argon-covered Cu(111) and Ag(111) by time-resolved two-photon photoemission, Phys. Rev. B **80**, 205425 (2009).

[21] N.-H. Ge, C. M. Wong, and C. B. Harris, Femtosecond studies of electron dynamics at interfaces, Acc. Chem. Res. **33**, 111 (1999).

[22] K. J. Gaffney, A. D. Miller, S. H. Liu, and C. B. Harris, Femtosecond dynamics of electrons photoinjected into organic semiconductors at aromatic-metal interfaces, J. Phys. Chem. B **105**, 9031 (2001).

[23] X.-Y. Zhu, Electronic structure and electron dynamics at molecule-metal interfaces: Implications for molecule-based electronics, Surf. Sci. Rep. **56**, 1 (2004).

[24] P. S. Kirchmann, P. A. Loukakos, U. Bovensiepen, and M. Wolf, Ultrafast electron dynamics studied with time-resolved two-photon photoemission: Intra- and interband scattering in C_6F_6/Cu(111), New J. Phys. **7**, 113 (2005).

[25] E. Varene, I. Martin, and P. Tegeder, Optically induced inter- and intrafacial electron transfer probed by two-photon photoemission: Electronic states of sexithiophene on Au(111), J. Phys. Chem. Lett. **2**, 252 (2011).

[26] M. Shibuta, N. Hirata, R. Matsui, T. Eguchi, and A. Nakajima, Charge separation at the molecular monolayer surface: Observation and control of the dynamics, J. Phys. Chem. Lett. **3**, 981 (2012).

[27] J. Zhao, M. Feng, D. B. Dougherty, H. Sun, and H. Petek, Molecular electronic level alignment at weakly coupled organic film/metal interfaces, ACS Nano **8**, 10988 (2014).

[28] P. M. Echenique, R. Berndt, E. V. Chulkov, T. Fauster, A. Goldmann, and U. Höfer, Decay of electronic excitations at metal surfaces, Surf. Sci. Rep. **52**, 219 (2004).

[29] S. S. Tsirkin, A. G. Borisov, and E. V. Chulkov, Green's function approach to the lifetimes of image potential resonances at metal surfaces, Phys. Rev. B **88**, 035449 (2013).

[30] D. C. Marinica, C. Ramseyer, A. G. Borisov, D. Teillet-Billy, J. P. Gauyacq, W. Berthold, P. Feulner, and U. Höfer, Effect of an Atomically Thin Dielectric Film on the Surface Electron Dynamics: Image-Potential States in the Ar/Cu(100) System, Phys. Rev. Lett. **89**, 046802 (2002).

[31] P. M. Echenique, J. M. Pitarke, E. V. Chulkov, and A. Rubio, Theory of inelastic lifetimes of low-energy electrons in metals, Chem. Phys. **251**, 1 (2000).

[32] K. Onda, B. Li, and H. Petek, Two-photon photoemission spectroscopy of TiO_2(110) surfaces modified by defects and O_2 or H_2O adsorbates, Phys. Rev. B **70**, 045415 (2004).

[33] W. A. Tisdale, M. Muntwiler, D. J. Norris, E. S. Aydil, and X.-Y. Zhu, Electron dynamics at the ZnO(10$\bar{1}$0) surface, J. Phys. Chem. C **112**, 14682 (2008).

[34] K. Takahashi, K. Ishibashi, Y. Kurahashi, M. Imamura, J. Azuma, and M. Kamada, Time-resolved two-photon photoemission study of silicon surface at initial stage of oxidation, Appl. Surf. Sci. **267**, 154 (2013).

[35] J.-C. Deinert, D. Wegkamp, M. Meyer, C. Richter, M. Wolf, and J. Stähler, Ultrafast Exciton Formation at the ZnO(10$\bar{1}$0) Surface, Phys. Rev. Lett. **113**, 057602 (2014).

[36] A. Argondizzo, X. Cui, C. Wang, H. Sun, H. Shang, J. Zhao, and H. Petek, Ultrafast multiphoton pump-probe photoemission excitation pathways in rutile TiO_2(110), Phys. Rev. B **91**, 155429 (2015).

[37] S. Otto and T. Fauster, Two-photon photoemission from CoO layers on Ir(100), J. Phys.: Condens. Matter **28**, 055001 (2016).

[38] F. Reinert and S. Hüfner, Photoemission spectroscopy—from early days to recent applications, New J. Phys. **7**, 97 (2005).

[39] S. Hüfner, Electronic structure of NiO and related 3d-transition-metal compounds, Adv. Phys. **43**, 183 (2006).

[40] M. Portalupi, L. Duò, G. Isella, R. Bertacco, M. Marcon, and F. Ciccacci, Electronic structure of epitaxial thin NiO(100) films grown on Ag(100): Towards a firm experimental basis, Phys. Rev. B **64**, 165402 (2001).

[41] H. Eckardt, L. Fritsche, and J. Noffke, Self-consistent relativistic band structure of the noble metals, J. Phys. F: Metal Phys. **14**, 97 (1984).

[42] A. Goldmann, V. Dose, and G. Borstel, Empty electronic states at the (100), (110), and (111) surfaces of nickel, copper, and silver, Phys. Rev. B **32**, 1971 (1985).

[43] F. Cinquini, L. Giordano, G. Pacchioni, A. M. Ferrari, C. Pisani, and C. Roetti, Electronic structure of NiO/Ag(100) thin films from DFT+U and hybrid functional DFT approaches, Phys. Rev. B **74**, 165403 (2006).

[44] I. O. Thomas and A. Fortunelli, Analysis of the electronic structure of ultrathin NiO/Ag(100) films, Eur. Phys. J. B **75**, 5 (2010).

[45] A. Schrön, M. Granovskij, and F. Bechstedt, Influence of on-site Coulomb interaction U on properties of MnO(001)2×1 and NiO(001)2×1 surfaces, J. Phys.: Condens. Matter **25**, 094006 (2013).

[46] A. Höfer, K. Duncker, M. Kiel, S. Förster, and W. Widdra, Laser-excited PEEM using a fully tunable fs-laser system, IBM J. Res. Dev. **55**, 1 (2011).

[47] K. Duncker, M. Kiel, and W. Widdra, Momentum-resolved lifetimes of image-potential states on Ag(001), Surf. Sci. **606**, L87 (2012).

[48] See Supplemental Material at http://link.aps.org/supplemental/10.1103/PhysRevB.97.085424 for a detailed description of the analysis procedure of the time-resolved 2PPE data .

[49] K. Marre and H. Neddermeyer, Growth of ordered thin films of NiO on Ag(100) and Au(111), Surf. Sci. **287**, 995 (1993).

[50] S. Großer, C. Hagendorf, H. Neddermeyer, and W. Widdra, The growth of thin NiO films on Ag(001) studied by scanning tunneling microscopy and spectroscopy, Surf. Interface Anal. **40**, 1741 (2008).

[51] K. L. Kostov, S. Polzin, S. K. Saha, O. Brovko, V. Stepanyuk, and W. Widdra, Surface-phonon dispersion of a NiO(100) thin film, Phys. Rev. B **87**, 235416 (2013).

[52] T. Bertrams and H. Neddermeyer, Growth of NiO(100) layers on Ag(100): Characterization by scanning tunneling microscopy, J. Vac. Sci. Technol. B **14**, 1141 (1996).

[53] I. Sebastian, T. Bertrams, K. Meinel, and H. Neddermeyer, Scanning tunneling microscopy on the growth and structure of NiO(100) and CoO(100) thin films, Faraday Discuss. **114**, 129 (1999).

[54] A. Dhaka, D. Sander, H.L. Meyerheim, K. Mohseni, E. Soyka, J. Kirschner, W. A. Adeagbo, G. Fischer, A. Ernst, and W. Hergert, Stress and structure at the NiO/Ag(001) interface, Phys. Rev. B **84**, 195441 (2011).

[55] M. Caffio, B. Cortigiani, G. Rovida, A. Atrei, and C. Giovanardi, Early stages of NiO growth on Ag(001): A study by LEIS, XPS, and LEED, J. Phys. Chem. B **108**, 9919 (2004).

[56] M. Caffio, A. Atrei, B. Cortigiani, and G. Rovida, STM study of the nanostructures prepared by deposition of NiO on Ag(001), J. Phys.: Condens. Matter **18**, 2379 (2006).

[57] M. Caffio, B. Cortigiani, G. Rovida, A. Atrei, C. Giovanardi, A. di Bona, and S. Valeri, Ultrathin nickel oxide films grown on Ag(001): A study by XPS, LEIS and LEED intensity analysis, Surf. Sci. **531**, 368 (2003).

[58] D. Alders, F. C. Voogt, T. Hibma, and G. A. Sawatzky, Nonlocal screening effects in 2p x-ray photoemission spectroscopy of NiO(100), Phys. Rev. B **54**, 7716 (1996).

[59] L. Sangaletti, L.E. Depero, and F. Parmigiani, On the non-local screening mechanisms in the 2p photoelectron spectra of NiO and La_2NiO_4, Solid State Commun. **103**, 421 (1997).

[60] See Supplemental Material at http://link.aps.org/supplemental/10.1103/PhysRevB.97.085424 for an alternative version to fit the data for 3 MLNiO/Ag(001).

[61] R. Smoluchowski, Anisotropy of the electronic work function of metals, Phys. Rev. **60**, 661 (1941).

[62] W. Altmann, V. Dose, and A. Goldmann, Momentum-resolved Bremsstrahlung Isochromat Spectroscopy of silver surfaces, Z. Phys. B **65**, 171 (1986).

[63] R. W. Schoenlein, J. G. Fujimoto, G. L. Eesley, and T. W. Capehart, Femtosecond dynamics of the $n = 2$ image-potential state on Ag(100), Phys. Rev. B **41**, 5436 (1990).

[64] G. A. Sawatzky and J. W. Allen, Magnitude and Origin of the Band Gap in NiO, Phys. Rev. Lett. **53**, 2339 (1984).

[65] S. Hüfner, J. Osterwalder, T. Riesterer, and F. Hulliger, Photoemission and inverse photoemission spectroscopy of NiO, Solid State Commun. **52**, 793 (1984).

[66] F. Reinert, P. Steinert, S. Hüfner, H. Schmitt, J. Fink, M. Knupfer, P. Sandl, and E. Bertel, Electron and hole doping in NiO, Z. Phys. B **97**, 83 (1995).

[67] X. Ren, I. Leonov, G. Keller, M. Kollar, I. Nekrasov, and D. Vollhardt, LDA + DMFT computation of the electronic spectrum of NiO, Phys. Rev. B **74**, 195114 (2006).

[68] J. Kuneš, V. I. Anisimov, S. L. Skornyakov, A. V. Lukoyanov, and D. Vollhardt, NiO: Correlated Band Structure of a Charge-Transfer Insulator, Phys. Rev. Lett. **99**, 156404 (2007).

[69] M. Däne, M. Lüders, A. Ernst, D. Ködderitzsch, W. M. Temmerman, Z. Szotek, and W. Hergert, Self-interaction correction in multiple scattering theory: Application to transition metal oxides, J. Phys.: Condens. Matter **21**, 045604 (2009).

[70] M. W. Cole, Electronic surface states of a dielectric film on a metal substrate, Phys. Rev. B **3**, 4418 (1971).

[71] C. B. Harris, N.-H. Ge, R. L. Lingle, J. D. McNeill, and C. M. Wong, Femtosecond dynamics of electrons on surfaces and at interfaces, Annu. Rev. Phys. Chem. **48**, 711 (1997).

[72] R. Newman and R. M. Chrenko, Optical properties of nickel oxide, Phys. Rev. **114**, 1507 (1959).

[73] P. M. Echenique and J. B. Pendry, Existence and detection of Rydberg states at surfaces, J. Phys. C: Solid State Phys. **11**, 2065 (1978).

[74] Ch. Reuß, I. L. Shumay, U. Thomann, M. Kutschera, M. Weinelt, T. Fauster, and U. Höfer, Control of the Dephasing of Image-Potential States by CO Adsorption on Cu(100), Phys. Rev. Lett. **82**, 153 (1999).

[75] M. Weinelt, C. Reuß, M. Kutschera, U. Thomann, I. L. Shumay, T. Fauster, U. Höfer, F. Theilmann, and A. Goldmann, Decay and dephasing of image-potential states due to surface defects and disorder, Appl. Phys. B **68**, 377 (1999).

[76] M. Roth, M. Pickel, W. Jinxiong, M. Weinelt, and T. Fauster, Electron Scattering at Steps: Image-Potential States on Cu(119), Phys. Rev. Lett. **88**, 096802 (2002).